Planning Stable and Efficient Paths for Articulated Mobile Robots On Challenging Terrains

Mohammad Norouzi, Jaime Valls Miro and Gamini Dissanayake
Centre for Autonomous Systems,
Faculty of Engineering and IT, University of Technology, Sydney (UTS),
Sydney NSW 2007, Australia
{mohammad.norouzi, jaime.vallsmiro, gamini.dissanayake}@uts.edu.au

Abstract

An analytical strategy to generate stable paths for a reconfigurable vehicle while also meeting additional navigational objectives is herein proposed. The work is motivated by robots traversing over challenging terrains during search and rescue operations, such as those equipped with manipulator arms and/or flippers. The proposed solution looks at minimizing the length of the traversed path and the energy expenditure in changing postures, yet also accounts for additional constraints in terms of sensor visibility (i.e arm configurations close to those orthogonal to the horizontal global plane which can afford a wider sensor view) and traction (i.e. flipper angles that provide the largest track-terrain interaction area). The validity of the proposed planning approach is evaluated with a multi-tracked robot fitted with flippers and a range camera at the end of a manipulator arm while navigating over two challenging 3D terrain data sets: one in a mock-up urban search and rescue arena (USAR), and a second one from a publicly available quasi-outdoor rover testing facility (UTIAS).

1 Introduction and Related Work

Autonomous mobile robots are necessarily required to find safe and feasible routes in their environment. This need is particularly relevant when operating over challenging terrains, where failure to avoid potential tip-over scenarios in dangerous regions can have catastrophic consequences. In fact these issues are not restricted to the autonomy aspects of mobile robot navigation, but also concern tele-operated robots or those controlled by on-board human operators carrying heavy payloads. Examples for these systems are numerous, from applications such as search and rescue [Kessens *et al.*, 2012], mobile manipulators [Morales *et al.*, 2013], agricultural vehicle [Grisso *et al.*, 2006], forestry industries [Papadopoulos and Rey, 2000] and planetary surface exploration [Iagnemma and Dubowsky, 2004].

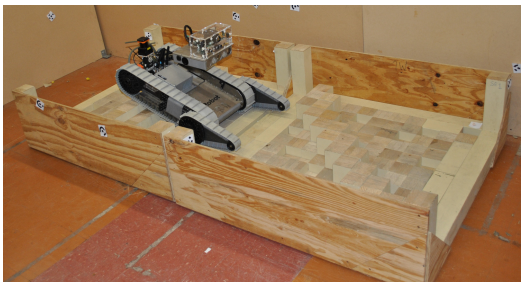

Figure 1: The Packbot robot with flippers and additional sensor head over a hill and diagonal step-fields.

Stability is one of the critical elements that bears a significant influence on the ability of a vehicle to traverse a given path. Assuming knowledge of the geometry of the terrain and the robot's inertial characteristics, a number of well studied stability measures can be employed to determine whether a vehicle will rest at a given location in the environment without tipping over. It is therefore apparent that for a reconfigurable rescue robot such as the one shown in Fig. 1 assuming safe postures should be an influential criterion to aid safe motion planning over rough terrain [Norouzi *et al.*, 2012].

The most influential tip-over stability measures are based on two criteria, the robot's centre of mass (CM) and the support polygon (SP) defined by the convex area spanned between the ground contact-points (CP). One of the most widely employed stability metric in robotics community is the force angle (FA) stability measure [Papadopoulos and Rey, 2000] which is briefly described in Section 2.1. Several algorithms have been proposed in the literature to address the stability and posture control of reconfigurable mobile robots on irregular terrain. An active control strategy for a reconfigurable wheel-legged mobile robot based on ground clearance, orientation, gradient stability margin, and wheel traction efficiency on irregular terrain is presented in [Freitas *et al.*, 2010]. A combination of the stability measure with an artificial potential field to obtain desired actuator values was used in [Besseron *et al.*, 2008]. Both of these works have employed FA measure to evaluate robot's stability.

An autonomous roll-over protection system for tracked robots with flippers using energy stability margin is presented in [Inoue *et al.*, 2008]. The track-terrain CP and the force distribution are evaluated using touch sensors which are embedded in the tracks. The performance of roll-over protection control is demonstrated on an unstable step. Getting feedback from CP under the tracks using force sensor arrays is however not easily adaptable to other robot models.

Traction optimisation has also been proposed as a constraint in the stability control of reconfigurable mobile robots, where a performance index considered the FA stability measure for each potential tip-over axis and the nominal values of the joints [Schenker *et al.*, 2003]. The minimisation of this performance index provided the most favourable configuration of the robot.

In [Norouzi *et al.*, 2012] our group proposed a study of the influence of a variable CM and the shape of the SP to plan safe traversable paths for the case of reconfigurable robots. A tracked robot in a basic kinematic configuration (without flippers) was fitted with a manipulator arm and a range camera to verify the result of the work. The fundamental motivation of that work considered a suitable arm angle that could afford the widest sensor view and keep stability within safe margins. The main drawback of the work was the partially heuristic nature of the proposed algorithm in choosing the desired postures of the search graph. In this work we present an alternative method in which we analytically compute a solution that optimizes the robot configuration in terms of visibility, traction and energy consumption in the presence of an overarching stability constraint over the length of a path. Hence, a closed-form optimization between neighbouring nodes in a graph is embedded within a traditional A* search algorithm to render a solution that computes the optimal path to follow. The A* search algorithm is employed in this work given its widespread use and in general optimal performance in graph searching. However, it should be noted that the proposed strategy is suitable for any cost-based graph search algorithm.

Furthermore, given that the proposed motion planning strategy is aimed at mobile platforms able to adapt their configuration, the iRobot Packbot robot model developed for [Norouzi *et al.*, 2012] has been extended in this work to consider both arm and flippers. This work does not consider uncertainty in the planning process. For details regarding these issues the reader is referred to [Norouzi *et al.*, 2013].

2 Stability Analysis Approach

2.1 Force Angle Stability Metric

Tracked vehicles usually operate gently over rough terrain and in general a quasi-static model can be safely assumed for the analysis of their stability [Iagnemma and Dubowsky, 2004]. The FA stability measure is detailed in [Papadopoulos and Rey, 2000], but it can be briefly explained based on the location of the CM over the robot SP as illustrated in Fig. 2. The n out-most CP between robot and terrain are marked

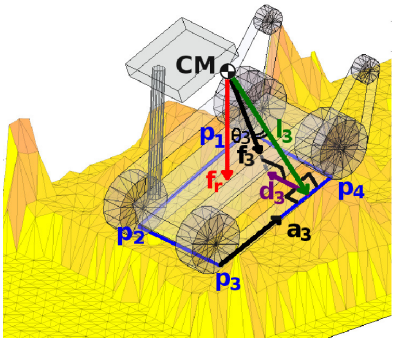

Figure 2: The 3D FA stability measure for $n = 4$ and $i = 3$. (CM's position has been shifted up and vectors scaled for easier visualization). Intuitively, the FA compactly describes the effect of the forces exerted on a vehicle's CM over each of the supporting axes defined by a vehicle sitting on a terrain.

in counter-clockwise order i.e. $\mathbf{p_i}$, $i = \{1,...,n\}$. The lines between every two consecutive CP and the resulting convex polygon will be referred to as the tip-over axes $\mathbf{a_i}$ and SP respectively. The vectors that intersect CM with each $\mathbf{a_i}$ are referred to as $\mathbf{l_i}$. Under quasi-static assumption, the net force $\mathbf{f_r}$ acting on the system's CM will come from the gravitational loading term. Then for a given tip-over axis $\mathbf{a_i}$, the components of $\mathbf{f_r}$ which acts about the tip-over axis is calculated as $\mathbf{f_i}$. The stability angle θ_i is computed as the angle between $\mathbf{f_i}$ and the tip-over axis normal $\mathbf{l_i}$. Critically, the FA stability measure is also sensitive to $\mathbf{d_i}$, the minimum length vector from $\mathbf{a_i}$ to $\mathbf{f_i}$, hence defining the ith stability measure β_i as:

$$\beta_i = \theta_i \ \|\mathbf{d_i}\| \ \|\mathbf{f_i}\|, \quad i = \{1,...,n\} \tag{1}$$

The example in Fig. 2 shows these derivations for $n = 4$ and $i = 3$. The overall robot's FA measure β is defined as:

$$\beta = min(\beta_i), \quad i = \{1,...,n\} \tag{2}$$

2.2 Robot Model

The robot model used to validate the result of this work is the multi-tracked iRobot Packbot robot depicted in Fig. 1. The mechanical structure consists of a skid-steer vehicle base, flippers (two small sub-tracks in the front) and an arm that carries a 2D pan-and-tilt unit equipped with several cameras and lights. Robot's coordinate frame convention is illustrated in Fig. 8b. It is clear that for these types of robots changing the angle of the arm and/or flippers (ϕ_a and ϕ_f) will change the location of the CM. Moreover, when the flippers are in contact with the terrain they change the shape of SP, which in turn has a more significant effect on the stability of the robot. More details about the robot's kinematic model and the effect of the mass distribution can be found in [Norouzi *et al.*, 2012].

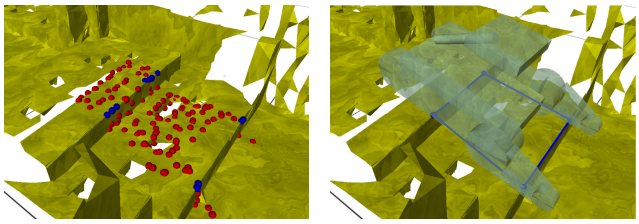

(a) *candidate points* in red and *touched points* in blue.

(b) The final SP, in this case resulting in 4 stability axes.

Figure 3: Projection of the robot's bottom surfaces on the gridded terrain to predict contact-points.

2.3 Contact-Points Prediction

To anticipate the stability measure, some works like [Liu and Liu, 2010] considered an ideal support polygon (ISP) i.e. the CP are assumed to be fixed under the sprockets of the robot. It will be illustrated through some experiments in Section 5.1 how this is a strong assumption for the case of highly unstructured terrains, where CP can lay anywhere along the robot's track and in general form a variable support polygon (VSP). In this work no ISP is assumed, and in this section the details of the process to derive the VSP of a robot on a terrain are presented.

The robot-terrain prediction algorithm is based on the mathematical description of the robot in a dynamics simulator. The Open Dynamics Engine (ODE) [Smith, 2005], a widely used physical rigid body dynamics simulator, has been employed in this work. A 3D model of the terrain has been constructed from the ranging data measured with the RGB-D camera on the head of the robot. The CP derivation scheme is predicated on calculating the projection of the robot's geometric underside on the points defining the terrain underneath.

Under the assumption of quasi-static equilibrium, the influence of gravitational forces for a given robot pose and configuration can be calculated as an iterative process. To that end, the concave polygon describing the vehicle (the robot's bottom surfaces considers the two flippers, two main tracks and a middle step) is first assumed to be sitting on a hypothetical plane with no *pitch* or *roll* at a given position and orientation in world coordinates.

The arm angle ϕ_a, flippers angle ϕ_f, coordinates of the centre point (x,y,z) and robot's orientation $(yaw, pitch, roll)$ - generally referred to as heading, elevation and banking - in the global reference frame fully describe the model. The 2D robot position (rx, ry, yaw) in the global reference frame and the angle of the arm and flippers joints (ϕ_a, ϕ_f) constitute the input variables. Then z of the hypothetical plane will be set to maximum z of the point which is in the terrain underneath. Supposing the initial values of $pitch = 0$, $roll = 0$, ODE simulates the behaviour of robot if it is dropped from this point and determines its primary position.

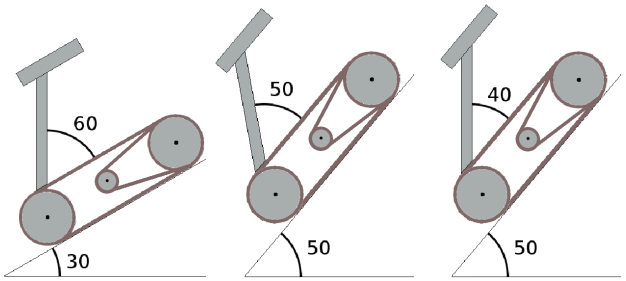

(a) $pitch = 30°$ $\phi_a nom = 60°$

(b) $pitch = 50°$ $\phi_a = 50°$

(c) $pitch = 50°$ $\phi_a nom = 40°$

Figure 4: Robot's *pitch* and nominal arm angles ϕ_a at two consecutive way points, (4a) and (4c), and the final arm configuration obtained by the reconfigurability function (4b).

The projection of the robot's bottom surfaces on the gridded terrain results in a set of *candidate points* (**P**) which are shown in Red in Fig. 3a. The point set located within a threshold distance set by the uncertainty in the grid modelling and rubbery track properties will be considered as *touched points* (**TP**) which are shown in Blue in Fig. 3a. As depicted in Fig. 3b, the outermost points from **TP** will become the ground CP needed to represent the SP of the vehicle when sitting on the terrain at that location. The tip-over axes $\mathbf{a_i}$ are defined as the segments that join the ground CP. A maximum of four possible CP are assigned to form the vertices of the SP, while at least three CP are needed for the pose to be regarded stable. Thus, the robot will be regarded stable at a given location if the resulting SP cause in $n \geq 3$ and $\beta > \beta_{min}$. Where n and β are defined in Eq. 1 and Eq. 2 respectively and β_{min} is the minimum safe stability margin.

3 Reconfigurability Objective Function

There are in general a large number of conflicting objectives that can play a significant role when planning paths in the context of realistic scenarios. For reconfigurable platforms in particular, favouring some nominal poses over others is very much dependent on the purpose of the application and the robot's kinematic constraints. For instance in search and rescue applications, a high position of the arm is generally preferred to afford wider sensor views, but this is in conflict with more stable posture which prefers lower arm position to keep CM as low as possible. In general, tracks and flippers should also remain in contact with the ground as much as possible to enhance locomotion [Okada *et al.*, 2011].

In this work, oriented towards search and rescue operations, the nominal configuration for the robot at a given point is assumed as:

1. The arm angle that affords the highest sensor height ($\phi_a nom$). The preferred robot posture is to keep the arm orthogonal with respect to the horizontal global coordi-

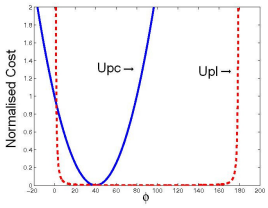

(a) Joint position and movement limitation costs.

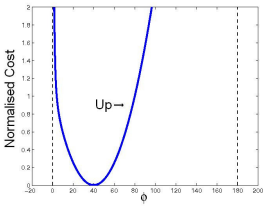

(b) Desired position cost functions.

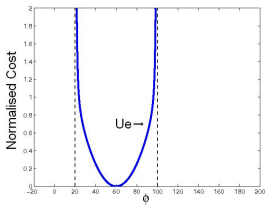

(c) Energy cost function.

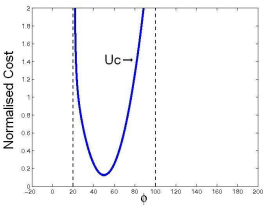

(d) The reconfiguration cost function.

Figure 5: Optimal arm joint configuration and its constrains.

nate frame to afford the widest possible field of view at all times.

2. The flippers angle that provides the largest track-terrain interaction area ($\phi_f nom$).

Moreover, increments in the joint configuration between way-points should also be considered to make sure the robot can follow the planned motions. Energy consumption is also a particularly relevant criteria when platforms are battery powered, so that changes in posture are kept to a minimum. The stability of the robot remains, however, the critical constraint so that if robot is ever found to be unstable, the optimality of any other parameters should be scarified to always satisfy the stability margin. The reconfiguration cost function of the robot U_c is proposed as

$$U_c = \sum_{i=1}^{n} U_i \tag{3}$$

where $n = 2$ is the number of robot's joints (i.e. for the Packbot model in this work $i \in \{1,2\}$ are chosen for flippers and arm joints respectively).

The U_i is the reconfiguration cost function for ith joint which is proposed as

$$U_i = Up_i + Ue_i \tag{4}$$

where Up_i is the cost associated to the desired position and Ue_i is an energy term associated to the reconfiguration of the joint. To better understand the meaning of these terms, the example depicted in Fig. 4 will be employed. For simplification only the arm angle is presented and the flippers are excluded from this case and they are supposed to be fixed at $\phi_f = 180^\circ$.

Suppose that the robot is sitting in a 30° ramp and current arm angle is $\phi_a = 60^\circ$ (Fig. 4a). The path planner has suggested the next way-point to move to as sitting in a 50° incline where the nominal joint position will be $\phi_a nom = 40^\circ$ (Fig. 4c). Supposing movement limitation of arm joint is $\phi_a min = 0^\circ$, $\phi_a max = 180^\circ$ and the maximum permitted arm movement between way-points has been set to $\Delta\phi_a max = 40^\circ$. It will be shown that by considering other costs, the optimal movement between these two way-points will be 50° as shown in Fig. 4b. It should be noted that the derivation of the proposed optimal solution is dependent on the joint's parameters, current angle and nominal position at a given time and location in the map, and therefore needs to be recalculated at each point again. As depicted in Fig. 5a, Up_i is composed of Upc_i a quadratic function on the joint cost, and a rational function Upl_i which depicts angle limitations.

$$Up_i = Upc_i + Upl_i \tag{5}$$

The quadratic function Upc_i is introduced to penalize joint positions that deviate from the nominal joint position with quadratically raising costs

$$Upc_i = Kpc_i\,(\phi_i - \phi_i nom)^2 \tag{6}$$

where ϕ_i and $\phi_i nom$ denote the angle of the ith joint, and its nominal position respectively. Kpc_i is a normalizing factor dependent on $\phi_i nom$ by

$$Kpc_i = \frac{1}{(\phi_i closer - \phi_i nom)^2} \tag{7}$$

where

$$\phi_i closer = \begin{cases} \phi_i min & |\phi_i min - \phi_i nom| < |\phi_i max - \phi_i nom| \\ \phi_i max & otherwise \end{cases} \tag{8}$$

i.e. $\phi_i closer$ indicates the joint limit closer to $\phi_i nom$ that makes Upc_i equal one, as depicted in Fig. 5a.

The rational function Upl_i in Eq. 5 is defined to account for joint constrains as

$$Upl_i = \begin{cases} Kpl_i \left(\left(\frac{1}{\phi_i - \phi_i min} \right)^2 + \left(\frac{1}{\phi_i max - \phi_i} \right)^2 \right) & \phi_i min < \phi_i < \phi_i max \\ \infty & elsewhere \end{cases} \tag{9}$$

where Kpl_i is a constant gain defined so that Upl_i will have a significant effect on Up_i near the extremes, whereas Upc_i will stay dominant in the rest of the domain, i.e. the minimum value for Up_i is near $\phi_i nom$. The domain of Upl_i function is limited to $\phi_i min < \phi_i < \phi_i max$, which will in turn limit the domain of the resulting function Up_i to this area as well. The resulting Up_i cost function is pictorially depicted in Fig. 5b.

Ue_i, depicted in Fig. 5c, is defined following a similar reasoning: it consist of both a quadratic and a rational term to restrict the general joint motion in postures between way-points, as well as to address the limitations of the maximum angular speed of each joints respectively

$$Ue_i = \begin{cases} Kec_i\,(\Delta\phi)^2 + Kel_i\left(\frac{1}{\Delta\phi_i max - |\Delta\phi_i|} - \frac{1}{\Delta\phi_i max}\right)^2 & |\Delta\phi_i| < \Delta\phi_i max \\ \infty & elsewhere \end{cases} \quad (10)$$

In the same way as Kpl_i, Kel_i is a small constant gain. $|\Delta\phi_i|$ is the absolute difference between two consecutive positions of the joint and $\Delta\phi_i max$ is the maximum possible gradient for the joint angle. Kec_i is a constant gain defined as

$$Kec_i = \left(\frac{1}{\Delta\phi_i max}\right)^2 \quad (11)$$

The suggested weighting factors defined by Eq. 7 and Eq. 11 can be suitably modified to place more emphasis on nominal positioning or energy expenditure in the motion of the joint.

The final joint reconfiguration cost function U_c for the example hereby described is depicted in Fig. 5d, where it can be analytically seen how the joint angle with the minimum cost at this location is 50°.

It is important to note that the energy term described in this work refers to "reconfiguration" changes, and it does not address the actual energy expenditure required to move the actual robot base over the given terrain. Moreover, while the cost terms are not directly derived from the robot's kinematic model, this is however considered in the calculation of the CM required by the FA measure, and in determining the joint movement limitations.

4 Planning Algorithm

The standard A* search algorithm ensures the optimality of the resulting path with respect to a given cost function $g(n)$. The cost of each possible node is evaluated and ranked by a priority function $f(n)$

$$f(n) = g(n) + \alpha\, h(n), \quad \alpha \in \{0,1\} \quad (12)$$

where $g(n)$ represents the accumulated cost from the *current* node n back to the start point, and $h(n)$ is an estimate of the remaining cost to get from node n to the target node. α is a weighting factor to speed up the searching process if an admissible heuristic function $h(n)$ exists. In the ordinary A* algorithm, $g(n)$ is usually based on Euclidean distances. In this section, a modification is proposed to also account for the additional parameters of interest, including energy expenditure, visibility, traction and an additional constraint to guarantee the stability of the path. The reconfiguration cost is optimized between two successor nodes as described in the previous Section, resulting in a 2D grid-based search space with two peculiarities: a) to ensure stability, a successor node will be added to *open* list or refreshed (gets new parent) if a safe transition is admissible by the reconfiguration ability of robot, and b) the cost function is modified to take into account the stability and reconfiguration cost, and will be biased towards poses with better visibility and traction.

Algorithm 1 Robot reconfiguration function

```
1:  function reconfig_robot()
2:      φa ← π/2, φf ← π/2
3:      ode_simulate(φa, φf)
4:      φa nom ← π/2 − pitch
5:      φf nom ← φf tangent
6:      minimize Uc
7:      ode_simulate(φa opt, φf opt)
8:      if (β > βmin) then
9:          return Uc(φa opt, φf opt) // Uc_min
10:     else   // find suboptimal stable arrangement
11:         search_direction ← sign(pitch)
12:         while (φa ≥ φa min & φa ≤ φa max) do
13:             φa ← φa − search_direction ∗ search_step
14:             φf ← φf tangent
15:             ode_simulate(φa, φf)
16:             if (β > βmin) then
17:                 return Uc(φa, φf)
18:             end if
19:         end while
20:         if (search_direction has not changed) then
21:             search_direction ← −search_direction
22:             go to 12
23:         end if
24:         return ∞ // no stable arrangement exists
25:     end if
26: end function
```

The reconfiguration cost described in Section 3 can be then reflected in the $g(n)$ term as

$$g(n) = \gamma Ud(n) + (1-\gamma)\,(Uc(n) + Us(n)), \quad 0 \le \gamma \le 1 \quad (13)$$

where $Ud(n)$ is the accumulated grid distance cost between successors (1 or $\sqrt{2}$), $Us(n)$ is the normalised stability cost, and $Uc(n)$ is the normalized robot reconfiguration cost according to Eq. 3. γ is a simple weighting factor to be able to place more emphasis on stability/reconfiguration or distance as desired.

The reconfiguration cost is known up to where the graph search space has been expanded, while the heuristic cost remains solely based on distance, as per the standard A*. In that regard, $h(n)$ remains an admissible heuristic for $f(n)$ in the same way it is for the standard A*.

Despite the proposed analytical function Uc for the reconfiguration cost, the optimization can not be expressed as a straightforward analytical problem. This is due to the stability constraint, and the fact that changes in the robot configuration may also change the robot's final pose in the terrain. In order to address these considerations the robot reconfiguration algorithm needs to be formulated as an iterative procedure, as summarized by Alg. 1. The algorithm first considers how the robot would sit on the terrain with a 90° arm and flippers configuration. The nominal configuration for

arm and flippers $(\phi_a nom, \phi_f nom)$ would be calculated based on the current robot's *pitch* and the interaction of the robot base and flippers with the terrain it is sitting on. The optimal configuration extracted by analytical minimization of Eq. 3 is considered as the initial candidate values. If the robot with the analytical optimum configuration is proved unstable, the arrangement will then deviate from the true optimum to a near-optimum, but stable one. If *pitch* angle is positive (robot nose up), the *search_direction* will be positive to search the postures with smaller arm angles first. This process will be repeated iteratively to find the minimum configuration that meets the threshold of stability criteria with the lowest cost. Otherwise, Uc will be regarded exceedingly large at that location in the map, effectively regarding the grid untraversable for planning purposes.

5 Experimental and Simulation Results

The effectiveness of the proposed planning technique has been evaluated using two challenging terrain data sets. The first one was obtained whilst operating the Packbot tracked robot in a reconfigurable mock-up $6m \times 8m$ USAR arena, whilst the second one is a freely available 3D data set from the UTIAS quasi-outdoor rover testing facility [Tong *et al.*, 2013]. First an experiment in the next section will be described to demonstrate the need of a stability analysis based on VSP versus the more simplistic ISP. Then an experimental validation over a smaller challenging terrain will demonstrate the approach and the close correlation between measured and simulated results. Finally, large simulation results over two extensive datasets will be used to validate the proposed algorithm.

5.1 Significance of ISP and VSP on stability prediction

The relevance of the proposed algorithm to compute the robot's VSP over the more simplistic ISP defined by the robot sprockets is verified in this section with experimental results in two representative environment settings. The robot was commanded to move slowly at a constant speed over two different impediments, a ramp and a flight of stairs as shown in Fig. 6a and Fig. 6b respectively, both with similar inclination. The arm configuration was fixed ($\phi_a = 10^\circ$ and $\phi_a = 50^\circ$) during each test. To allow for maximum traction, flippers were repositioned to remain tangential to the terrain ($\phi_f nom$).

Pitch increased from zero (robot on flat terrain) to approximately 30° and 25° over the ramp and stairs respectively. There was no significant *roll* and it is therefore omitted from the results. IMU data, localization and robot's posture was recorded during the tests and FA stability margins were then calculated off-line using real IMU data and robot posture from the experiment while assuming an ISP, and using the robot localization information, robot posture and 3D environment data from the experiment, and the VSP attained from

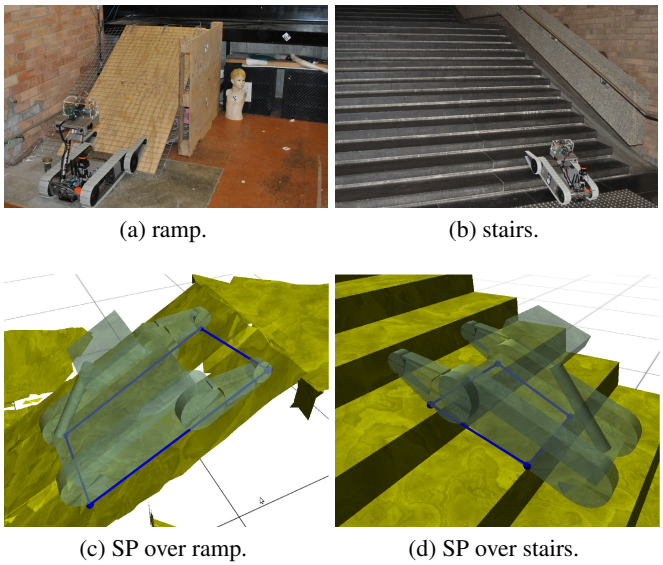

(a) ramp. (b) stairs.

(c) SP over ramp. (d) SP over stairs.

Figure 6: Ramp and stairs and the shape of the support polygons (SP).

the 3D ODE simulations of the robot in the environment, as described in section 2.3.

The results of calculating FA margins for an ideal and a variable SP and a fixed arm configuration of $\phi_a = 10^\circ$ are shown in Fig. 7a and Fig. 7b. It can be seen how computing stability solely based on inclination data and an assumption of ISP, as in [Roan *et al.*, 2010], will result in relatively similar safe tip-over margins for both topologies (shown in black in the figures). However, as illustrated in Fig. 6c and Fig. 6d the shape of the SP at these two places is quite different despite similar average *pitch* angles. *Pitch* oscillates in the transition between two steps i.e. at the instances when the robot was loosing contact with the rear step until the time new contact was made with the next step. The SP is therefore smaller on the stairs when compared to that on the ramp. As such, when considering stability margins, the effect of a VSP on a ramp is confidently positive, but it borders on instability on the stairs.

This is further observed in the second test where the robot was driven over both topologies with a different arm configuration, ($\phi_a = 50^\circ$), resulting in a higher CM position. The results indicates how despite lower stability margins the robot was able to come up the ramp safely, yet it proved to be unstable over the stairs and was about to tip-over around the transitions between steps - it and had to be manually handled to return it back to the terrain to prevent a fatal crash. Fig. 7c and Fig. 7d depict FA margins for the ramp and stairs respectively. VSP reflects how FA measures for the ramp are always positive while at times reaches negative values over the stairs. On the other hand, stability measures based on ISP remain always positive for both topologies and are not able to accurately predict instability over stairs. *Pitch* angle evolu-

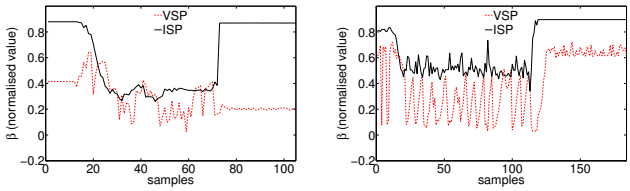

(a) β ($\phi_a = 10$).

(b) β ($\phi_a = 10$).

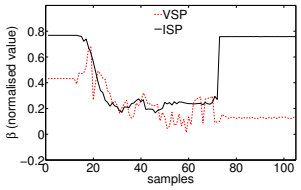

(c) β ($\phi_a = 50$).

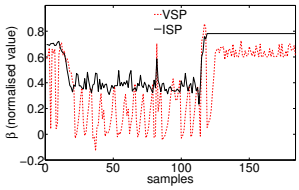

(d) β ($\phi_a = 50$).

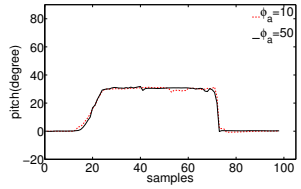

(e) *pitch*.

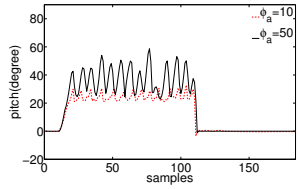

(f) *pitch*.

Figure 7: FA stability measure and *pitch* in two trials over ramp (left) and stairs (right).

tion over the stair test can be seen in Fig. 7f, clearly showing sudden crests where tip-over was starting to occur.

5.2 Planning over two step-fields

The aim of this experiment was to evaluate the performance of the proposed algorithm in planning over a known step-field arrangements consisting of adjacent diagonal and hill configurations, as depicted in Fig. 1. In addition to the robot's position, the path way-points also include the robot's posture at the desired locations.

Setting the start point in the beginning of the first step-field and the goal node at the end of second one, a relatively straight trajectory with 32 way-points was generated off-line running the proposed planning algorithm in the ODE simulator. Each way-point includes 2D position of of robot on the grid as well as the flippers and arm angles in that location.

The robot was then placed at the same starting position in the real arena, and the resulting way-points were loaded to a controller to follow the suggested trajectory and reconfigure the robot to the corresponding planned posture at the way-points. A localizer running of 2D range data from an auto-levelled laser scanner was used to derive an estimate of the robot pose (x, y, yaw) with a previously built 3D mesh of the arena depicted in Fig. 8. Data was recorded at 376 locations along the path traversed by the robot. A side view of a subset of the path with the robot arrangements suggested by the

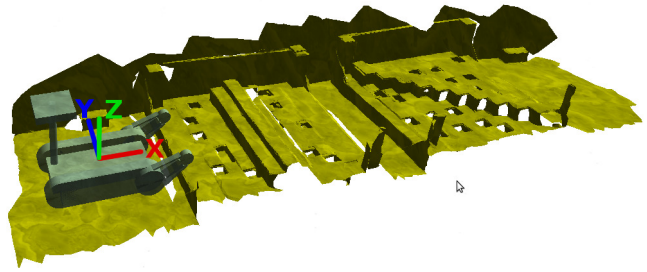

(a) The 3D meshed model.

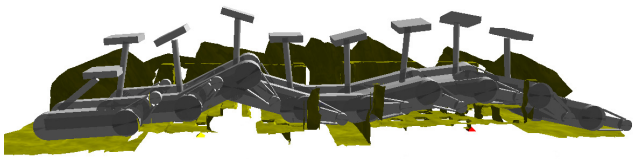

(b) The side view of robot configurations.

Figure 8: Hill and diagonal step-fields and their 3D models. A photo of the real step-fields is illustrated in Fig. 1

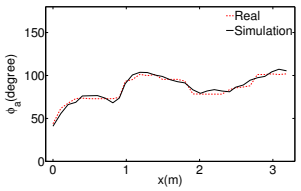

(a) arm.

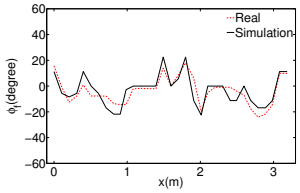

(b) flippers.

Figure 9: Measured and set-point configurations.

planner is depicted in Fig. 8b - omitted in some places to increase clarity.

The recorded angles of the arm and flippers joints are shown in Fig. 9b and Fig. 9a respectively. The robot inclination information measured by IMU is depicted in Fig. 10b and Fig. 10a. A comparison between the measured and predicted vehicle *pitch* and *roll* derived from the ODE simulation at these locations was carried out to indirectly assess the proposed algorithm for calculating contact surfaces and stability measures. The results presented in the figures Fig. 10a and Fig. 10b clearly indicate a close correlation between the real values and those inferred from the derivation of the ODE. The comparison between the measured and the values set in the way-point for flippers and arm angles indicate a reasonable controller performance as depicted in Fig. 9b and Fig. 9a respectively.

5.3 Path Planning in an indoor USAR arena

In a practical scenario such as search and rescue, prior knowledge of the terrain can not be assumed to be available, and the robot needs to create the coverage map as it navigates further. As detailed in [Norouzi *et al.*, 2012], when only partial in-

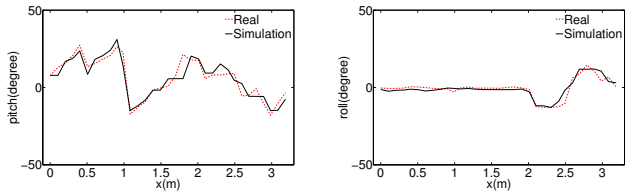

(a) *pitch*. (b) *roll*.

Figure 10: Measured and predicted inclinations.

	Nominal	Optimal	Improvement
arm	909.73	673.93	25.92%
flippers	1323.41	888.27	32.88%

Table 1: Overal energy costs ($\sum_{i=1}^{n} Ue_i$) for the arm and flippers trajectories shown in Fig. 12.

formation from the surrounding area is available, path planning in an exploratory setting is needed. The outcomes of the proposed algorithm are first presented in such a scenario in Fig. 11a, where the robot configurations have been omitted in some places to increase clarity.

The proposed optimal configuration planner results in smoother arm trajectories as depicted in Fig. 12a and Fig. 12b, where comparison between the nominal trajectories planned by the nominal high-visibility stable paths planner [Norouzi *et al.*, 2012] and the optimal postures obtained by the proposed planner are shown. Table. 1 summarizes the energy reconfiguration costs of the nominal and proposed optimal posture trajectories, showing improvement of 25.92% and 32.88% for arm and flippers respectively.

The effect of the proposed planner is further illustrated on the USAR arena depicted in Fig. 11b in a comparison with the standard A*. For this experiment complete knowledge of the terrain was assumed. In order to make a fair comparison between the two planners a pre-processing algorithm was first applied to the terrain model to label out obvious untraversable areas, e.g. walls and markedly steep slopes. Results show the path derived from the original A* in blue. A stability analysis of this path found sections (shown in red) where the robot was not stable for the fixed vertical arm and flipper pose assumed during a path with no reconfigurability. The values of the stability measures (βs) are plotted in Fig. 13a, where negative values corresponding to the red robot poses along the trajectory.

The most stable with lowest reconfiguration cost path (α and γ equal to zero in Eq. 12 and Eq. 13 respectively) found by the modified A* is also shown with an outline of the robot pose at regular intervals. It illustrates how an alternative path was preferred by going up the ramp and avoiding the steps and the step-fields, hence opting for more stable and lower reconfiguration cost poses over those leading to shorter paths.

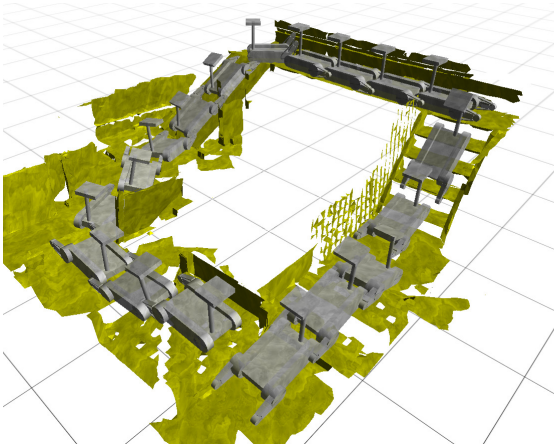

(a) Exploratory scenario.

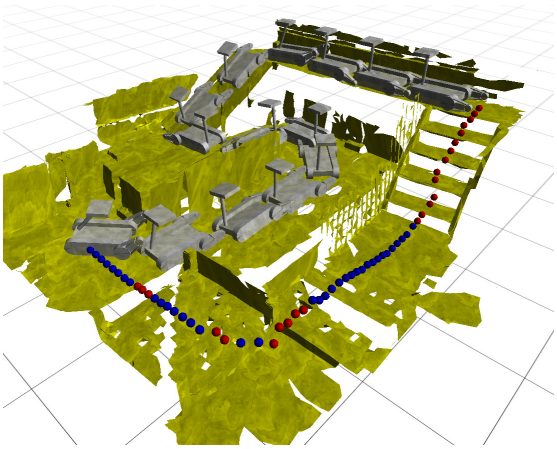

(b) Full map.

Figure 11: Results of stability criterion in A* algorithm in USAR arena. In Fig. 11b the standard A* path is shown in blue, with unstable regions are depicted in red. Robot poses derived from the most stable with lowest reconfiguration cost A* path are outlined in light Gray.

5.4 Planning on a Planetary Rover Testing Arena

In this example the proposed algorithm is tested with 3D terrain data collected from the quasi-outdoor UTIAS rover testing arena [Tong *et al.*, 2013]. The UTIAS testing facility consists of a large dome structure, which covers a workspace area 40m in diameter. A 3D model of environment has been obtained using an infrastructure-based ground-truth localization system suitable for deployment in large work-site environments. The set-up is able to provide full 6D relative localization for three-dimensional LRFs with centimetre-level accuracy in translation, and half degree accuracy in orientation. Fig. 14a depicts a panoramic image of the UTIAS indoor rover testing facility, with the rover used to gather the data in the foreground, and three of the four reflective signs used by the ground-truth localization system mounted on the dome structure in the background. These datasets are avail-

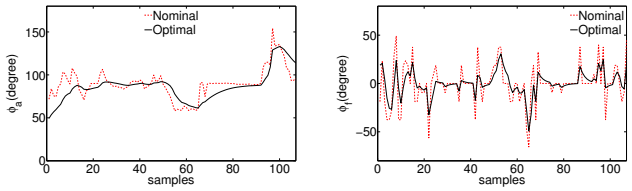

(a) arm. (b) flippers.

Figure 12: Arm and flippers trajectories planned by a high-visibility stable path planner only, and with the additional posture optimisation proposed in this work.

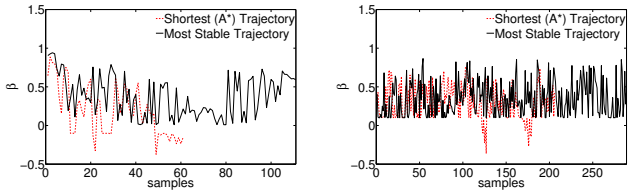

(a) USAR arena. (b) UTIAS arena.

Figure 13: Stability metrics (βs) along the trajectories.

able online and for more information, the reader is referred to [Tong *et al.*, 2013].

Given the large dimension of the UTIAS arena in relation to the robot's size, path planning results are illustrated from a top-down view in Fig. 14b.Gray-scale colour coding indicates height of the terrain from 0 to 2.76*m*. A pre-processing algorithm based on terrain gradients was first applied to the model to label out obviously untraversable steep slopes, shown in dark brown. This effectively filtered out regions with more than 56° gradient which corresponds to the critically unstable point in *pitch* for a robot sitting flat with an arm configuration at 90°, i.e. the highest visible point in flat terrain.Results show the path derived from standard shortest A* in blue, where unstable points with a fixed configuration with 90° arm and flipper are shown in red. The proposed shortest stable and most stable paths are shown in black and yellow respectively. It can be seen how the standard and proposed A* paths more or less coincided up to the middle of the second hill (in lighter Gray), where robot's stability appears compromised for a fixed configuration vehicle. The values of the stability measures (βs) are plotted in Fig. 13b, where negative unstable values correspond to the red spots along the trajectory.

6 Conclusion and Future Work

A strategy for motion planning in challenging environments for reconfigurable robots such as those equipped with manipulator arms and/or flippers has been presented in this article. The algorithm is able to minimise the length of the traversed path and optimise over conflicting robot reconfiguration cost

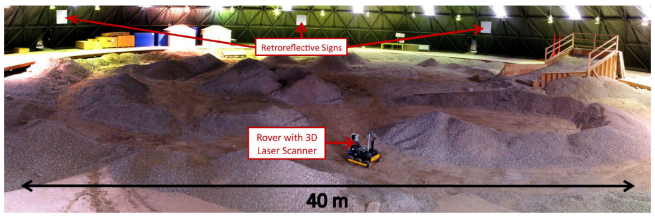

(a) UTIAS arena.

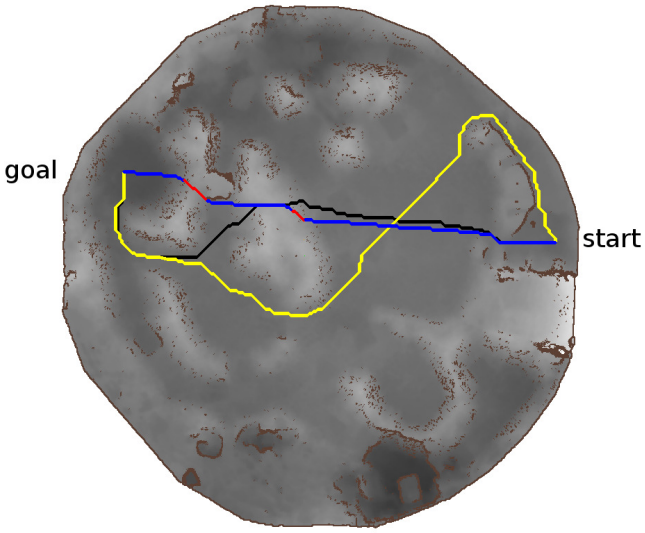

(b) Planning results.

Figure 14: Results of stability criterion in UTIAS arena. a) A panoramic image of the UTIAS indoor rover testing facility, with the rover used to gather the data in the foreground. b) Gray-scale colour coding indicates height of the terrain from 0 to 2.76m. Standard A* path is shown in blue with unstable fixed configuration poses in red. The proposed optimal and most stable reconfiguration trajectories are shown in black and yellow.

between consecutive graph nodes in terms of visibility, traction and energy consumption in the presence of stability constraint and limitations in the robot's joint movement. Experimental and simulation results with a reconfigurable tracked robot model have been presented to validate the proposed approach over more simplistic approaches that do not account for reconfiguration in the path estimates. The need for stability computations based on VSP when planning for safer navigational routes have also been established through experiments over two common indoor obstacles i.e. ramps and stairs.

References

[Besseron *et al.*, 2008] G. Besseron, Ch. Grand, F. Ben Amar, and Ph. Bidaud. Decoupled control of the high mobility robot hylos based on a dynamic stability margin. In *Proc. IEEE/RSJ International Conference on Intelligent Robots and Systems (IROS)*, pages 22–23, Nice, France, September 2008.

[Freitas *et al.*, 2010] G. Freitas, G. Gleizer, F. Lizarralde, and L. Hsu. Kinematic reconfigurability control for an environmental mobile robot operating in the amazon rain forest. *Journal of Field Robotics*, 27(2):197–216, 2010.

[Grisso *et al.*, 2006] Robert Grisso, John Perumpral, and Frank Zoz. An empirical model for tractive performance of rubber-tracks in agricultural soils. *Journal of Terramechanics*, 43:225–236, 2006.

[Iagnemma and Dubowsky, 2004] Karl Iagnemma and Steven Dubowsky. *Mobile Robot in Rough Terrain*, volume 12. Springer Tracts in Advanced Robotics, Berlin, Germany, 2004.

[Inoue *et al.*, 2008] Daisuke Inoue, Kazunori Ohno, Shinsuke Nakamura, and Satoshi Tadokoro. Whole-body touch sensors for tracked mobile robots using force-sensitive chain guides. In *Proc. IEEE International Workshop on Safety, Security and Rescue Robotics, Sendai, Japan, October 2008*, 2008.

[Kessens *et al.*, 2012] Chad C. Kessens, Daniel C. Smith, and Philip R. Osteen. A framework for autonomous self-righting of a generic robot on sloped planar surfaces. In *Proc. IEEE International Conference on Robotics and Automation (ICRA)*, pages 4724–4729, Minnesota, USA, May 2012.

[Liu and Liu, 2010] Yugang Liu and Guangjun Liu. Interaction analysis and online tip-over avoidance for a reconfigurable tracked mobile modular manipulator negotiating slopes. *IEEE/ASME Transactions on Mechatronics*, 15(4):623–635, August 2010.

[Morales *et al.*, 2013] Jesus Morales, Jorge L. Martinez, Anthony Mandow, Javier Seron, and Alfonso J. Garcia-Cerezo. Static tip-over stability analysis for a robotic vehicle with a single-axle trailer on slopes based on altered supporting polygons. *IEEE/ASME Transactions on Mechatronics*, 18(2):697–705, April 2013.

[Norouzi *et al.*, 2012] Mohammad Norouzi, Jaime Valls Miro, and Gamini Dissanayake. Planning high-visibility stable paths for reconfigurable robots on uneven terrain. In *IEEE/RSJ International Conference on Intelligent Robots and Systems (IROS)*, pages 2844–2849, Portugal, October 2012.

[Norouzi *et al.*, 2013] Mohammad Norouzi, Jaime Valls Miro, and Gamini Dissanayake. A statistical approach for uncertain stability analysis of mobile robots. In *Proc. IEEE International Conference on Robotics and Automation (ICRA)*, pages 191–196, Karlsruhe, Germany, May 2013.

[Okada *et al.*, 2011] Yoshito Okada, Keiji Nagatani, Kazuya Yoshida, Satoshi Tadokoro, Tomoaki Yoshida, and Eiji Koyanagi. Shared autonomy system for tracked vehicles on rough terrain based on continuous three-dimensional terrain scanning. *Journal of Field Robotics*, 28(6):875–893, 2011.

[Papadopoulos and Rey, 2000] Evangelos Papadopoulos and Daniel A. Rey. The force angle measure of tipover stability margin for mobile manipulatiors. *Vehicle System Dynamics*, 33(1):29–48, January 2000.

[Roan *et al.*, 2010] Philip R. Roan, Aaron Burmeister, Amin Rahimi, Kevin Holz, and David Hooper. Real-world validation of three tipover algorithms for mobile robots. In *Proc. IEEE International Conference on Robotics and Automation (ICRA)*, pages 4431–4436, Anchorage, Alaska, USA, May 2010.

[Schenker *et al.*, 2003] P. Schenker, T. Huntsberger, P. Pirjanian, S. Dubowsky, K. Iagnemma, and V. Sujan. Rovers for agile, intelligent traverse of challenging terrain. In *Proc. of the 7th International Symposium on Artificial Intelligence, Robotics and Automation in Space (i-SAIRAS)*, pages 1–10, Nara, Japan, May 2003.

[Smith, 2005] R. Smith. *Open Dynamics Engine*, 2005.

[Tong *et al.*, 2013] Chi Hay Tong, David Gingras, Kevin Larose, Timothy D Barfoot, and Erick Dupuis. The canadian planetary emulation terrain 3D mapping dataset. *The International Journal of Robotics Research*, 32(4):389–395, 2013.